The Astrophysical Journal, 675:604–613, 2008 March 1

RELATIVISTIC EFFECTS IN EXTREME MASS RATIO GRAVITATIONAL WAVE BURSTS

Nicolás Yunes
Institute for Gravitational Physics and Geometry, Center for Gravitational Wave Physics, Department of Physics, Pennsylvania State University, University Park, PA 16802

Carlos F. Sopuerta
Department of Physics, University of Guelph, Guelph, ON N1G 2W1, Canada

and

Louis J. Rubbo and Kelly Holley-Bockelmann
Center for Gravitational Wave Physics, Pennsylvania State University, University Park, PA 16802
Received 2007 April 19; accepted 2007 November 7

ABSTRACT

Extreme mass ratio bursts (EMRBs) have been proposed as a possible source for future space-borne gravitational wave detectors, such as the *Laser Interferometer Space Antenna* (*LISA*). These events are characterized by long-period, nearly radial orbits of compact objects around a central massive black hole. The gravitational radiation emitted during such events consists of a short burst, corresponding to periapse passage, followed by a longer, silent interval. In this paper we investigate the impact of including relativistic corrections to the description of the compact object's trajectory via a geodesic treatment, as well as including higher order multipole corrections in the waveform calculation. The degree to which the relativistic corrections are important depends on the EMRB's orbital parameters. We find that relativistic EMRBs ($v_{\rm max}/c > 0.25$) are not rare and actually account for approximately half of the events in our astrophysical model. The relativistic corrections tend to significantly change the waveform amplitude and phase relative to a Newtonian description, although some of this dephasing could be mimicked by parameter errors. The dephasing over several bursts could be of particular importance not only to gravitational wave detection, but also to parameter estimation, since it is highly correlated to the spin of the massive black hole. Consequently, we postulate that if a relativistic EMRB is detected, such dephasing might be used to probe the relativistic character of the massive black hole and obtain information about its spin.

Subject headings: black hole physics — Galaxy: nucleus — gravitational waves — stellar dynamics

Online material: color figures

1. INTRODUCTION

Low-frequency (10^{-5} Hz $\lesssim f \lesssim 0.1$ Hz) gravitational wave interferometers, such as the proposed *Laser Interferometer Space Antenna* (*LISA*; Bender et al. 1998; Danzmann & Rüdiger 2003; Sumner & Shaul 2004), will open a completely new window to the universe. Through observations of low-frequency gravitational radiation we will be able to witness the inspiral and merger of massive black hole binaries; the inspiral of compact objects into massive black holes; and millions of quasi-stationary compact galactic binaries. Recently, a new source of low-frequency gravitational radiation has been suggested: extreme mass ratio bursts (EMRBs; Rubbo et al. 2006a, 2006b).

EMRBs consist of a stellar-mass compact object (SCO) orbiting a massive black hole (MBH) of 10^4–10^8 $M_\odot$ with orbital periods greater than $T_{\rm cut} = 3 \times 10^4$ s. The defining orbital period cutoff is derived from *LISA*'s lower frequency limit of $f_{\rm cut} = 3 \times 10^{-5}$ Hz. Systems with orbital periods less than $T_{\rm cut}$ will radiate continuously inside the *LISA* band. Such continuous systems are more appropriately categorized as extreme mass ratio inspirals (EMRIs) and have been studied extensively elsewhere: recent estimations of the event rate are given by Gair et al. (2004) and Hopman & Alexander (2006); a discussion on a possible EMRI background is given by Barack & Cutler (2004a). Accounts on the theoretical description of EMRIs can be found in the reviews by Poisson (2004) and Glampedakis (2005), while the recent review by Amaro-Seoane et al. (2007) describes the astrophysical and detection applications.

Although EMRB events are distinct from EMRI events, their evolutionary track could be connected. In the burst scenario, the SCO orbits the MBH emitting a beamed burst of gravitational radiation during pericenter passage. The emitted radiation carries away energy and angular momentum from the system so that after multiple pericenter passages the orbital period decreases, and possibly the system becomes an EMRI. However, this evolutionary track is most likely disrupted by scattering interactions with other stars and/or if the SCO plunges directly into the central MBH on one of its passages.

The EMRB event rate has recently been investigated using simplified galactic models and data analysis techniques (Rubbo et al. 2006a, 2006b; Hopman et al. 2006). Using a density profile described by an η-model (Tremaine et al. 1994), Rubbo et al. (2006a, 2006b) suggested an event rate of $\sim$15 yr^{-1} for events with signal-to-noise ratios (S/Ns) greater than 5 out to the Virgo Cluster. When mass segregation and different inner cusp models are considered, the predicted rate decreases by an order of magnitude (Hopman et al. 2006). These preliminary studies were aimed at understanding if EMRB event rates are interesting for low-frequency gravitational wave detectors such as *LISA*. More work is still needed to improve the predicted event rate in the context of realistic galaxies, where the role of nonequilibrium dynamics, anisotropy, complex star formation histories, substructure, and nonsphericity may act to change the rate from these fiducial estimates by orders of magnitude (Holley-Bockelmann & Sigurdsson 2006; Rubbo et al. 2006a, 2006b).

In addition to the astrophysical uncertainties, there are no investigations of the impact of relativistic corrections to EMRB dynamics. All EMRB studies have been carried out in a *quasi-Newtonian* framework. In this framework, one uses the Newtonian equations of motion and extracts the gravitational waveforms by means of the *quadrupole formula*. This approximation ignores the black hole nature of the central potential, including the black hole's rotation (spin), and is technically valid only for orbits with nonrelativistic velocities. However, a considerable number of EMRBs are characterized by large pericenter velocities ($v_p \gtrsim 0.25c$) and these *relativistic* EMRBs should produce gravitational wave signals with larger S/Ns, as we show later.

In this paper we do not consider the issue of EMRB event rates, but instead we study the effects of relativistic corrections to such events. For extreme mass ratio systems a simple way of introducing relativistic corrections is by using the so-called *semirelativistic* approximation introduced by Ruffini & Sasaki (1981) and used recently in the context of EMRIs by Gair et al. (2005, 2006). In this approximation, the MBH and surrounding area are modeled using the Kerr solution to Einstein's field equations, which describes a stationary spinning black hole (the Schwarzschild solution corresponds to the nonspinning case). The SCO is considered to be a pointlike object (neglecting its own self-gravity) whose trajectory is described by a geodesic of the Kerr spacetime. In other words, relative to previous work, we have replaced the Newtonian equations of motion by relativistic geodesic equations of motion.

The relativistic description introduces effects such as orbital precession and frame dragging, but it does not account for effects due to the gravitational field induced by the SCO. These effects, for example, lead to changes in the (geodesic) constants of motion due to radiation reaction. Even though these effects introduce errors that scale with the system's mass ratio (e.g., see Glampedakis 2005), they cannot be neglected for EMRIs. This is because in the late stages of the EMRI the SCO spends a substantial fraction of cycles in the strong-field region of the MBH. On the other hand, in the case of EMRBs, the SCO slingshots around the MBH and its interaction time during pericenter passage is relatively small ($<10^5$ s). Radiation reaction effects can then be neglected in EMRBs, since the radiation reaction timescale is always much larger than the period of pericenter passage.

In this paper we also improve on the semirelativistic approximation by using a more precise gravitational wave extraction procedure. The procedure employed is the multipole-moment wave generation formalism for slow-motion objects with arbitrarily strong internal gravity (Thorne 1980). We consider terms up to the mass-octopole and current-quadrupole multipoles, thus improving on the mass-quadrupole analysis of Rubbo et al. (2006a, 2006b) and Hopman et al. (2006). Higher multipoles will become important if the system becomes even more relativistic, but pericenter velocities for EMRBs are typically small to moderate relative to the speed of light (typically $0.1 \lesssim v_p/c \lesssim 0.5$). Such higher multipolar corrections were taken into account for EMRIs by Babak et al. (2007), but for those sources the phase evolution must be tracked very accurately, requiring techniques from black hole perturbation theory (Poisson 2004; Glampedakis 2005) that we do not consider here.

The study of the relativistic corrections considered in this work leads to the following conclusions. First, we find that relativistic effects are significant for approximately 50% of the orbits contained in the EMRB phase space considered by Rubbo et al. (2006a, 2006b). These relativistic EMRB orbits differ from their Newtonian counterparts in such a way that the associated waveforms present a noticeably different structure. In particular, we find that there is a dephasing relative to Newtonian waveforms that is due to precessional effects and depend strongly on the MBH spin. These findings show that EMRB events are relativistic enough that they should be treated accordingly, as was previously found for EMRIs (Glampedakis 2005).

Second, we find that the corrections to the trajectories affect the waveforms much more than the corrections in the waveform generation over several bursts. For example, for a given relativistic trajectory, we find that the difference between the S/N of a waveform obtain from the quadrupole formula to that obtained from the quadrupole-octopole formula is of the order of 10% (depending on the location of the observer.) On the other hand, using the same waveform generation formula (quadrupole or quadrupole-octopole), the difference between the S/N of a Newtonian waveform to that of a Kerr waveform is of the order of 100%. These findings show that modeling EMRB waveforms with a quasi-Newtonian treatment might not be sufficient for certain data analysis applications.

Third, we find that the relativistic corrections accumulate with multiple bursts and, thus, they may have an important impact in improving the S/N. It is also conceivable that such corrections might be important for parameter estimation studies and, perhaps, may be used to determine or bound the spin of the MBH if a high-S/N event is detected. Along this same lines, if parameters can be determined accurately enough, it might also be possible to use EMRB measurements to test deviations from general relativity. We must note, however, that changing the orbital parameters in Newtonian waveforms could somewhat mimic some of the relativistic corrections, but a detailed Fisher analysis of such effects is beyond the scope of this paper.

The remainder of this paper is divided as follows: § 2 deals with the dynamics of EMRBs in the semirelativistic approximation and justifies the use of this approximation for these systems; § 3 reviews the inclusion of higher order multipolar corrections to the waveform generation formalism; § 4 describes the numerical implementation of the equations of motion and the initial data used; § 5 compares the orbital trajectories and waveforms; and § 6 concludes and points to future research.

In this paper we denote the MBH mass by $M_\bullet$ and its *gravitational radius* by $R_\bullet = 2GM_\bullet/c^2$, where c is the speed of light and G the Newtonian gravitational constant. To simplify some expressions we normalize masses with respect to $M_{\rm MW} = 4 \times 10^6\ M_\odot$, which is of the same magnitude as the mass of the MBH at the center of the Milky Way (Ghez et al. 2005). The gravitational radius can then be written as

$$R_\bullet = (3.82 \times 10^{-7}\ \text{pc}) \frac{M_\bullet}{M_{\rm MW}}. \quad (1)$$

2. EMRB DYNAMICS

In this section we discuss the description of the orbital motion. Newtonian dynamics usually provides an adequate description of many astrophysical sources of gravitational waves, at least from a qualitative point of view. However, for certain gravitational wave sources, such a description is insufficient and relativistic effects have to be considered. For EMRB sources with pericenter distances $r_p > 4R_\bullet$ and velocities $v_p/c < 0.5$, the semirelativistic approximation to the equations of motion, in combination with a multipolar description of the gravitational radiation, can adequately model the dynamics and gravitational radiation, as we argue below.

The semirelativistic approximation treats the motion of the SCO in the point-particle limit as a geodesic of the MBH geometry, which is justified based on the small mass ratios associated with these systems. In this work, we adopt Cartesian Kerr-Schild

coordinates, $\{t, x^i\}$ ($i = 1, 2, 3$), in which the MBH geometry is time-independent, reflecting its stationary character, and tends to a flat-space geometry in Cartesian coordinates far from the MBH. We denote the geodesic trajectory by $z^i(t)$, its spatial velocity by $v^i(t) = dz^i/dt$, and its spatial acceleration by $a^i(t) = dv^i/dt$. The latter, in such a coordinate system, and by virtue of the geodesic equations of motion, has the following form (e.g., see Marck 1996):

$$a^i = F^i[v^j; g_{\mu\nu}, \partial_j g_{\mu\nu}], \tag{2}$$

where $g_{\mu\nu}$ ($\mu, \nu = 0, 1, 2, 3$) are the spacetime components of the MBH metric. These equations describe the influence of the spacetime curvature produced by the MBH and approach the Newtonian equations of motion in the regime where $v/c = |v^i|/c \ll 1$ and $GM_\bullet/(c^2 r) \ll 1$ ($r = |x^i|$).

The effects from the self-gravity of the SCO can be neglected. To see this, consider the (Keplerian) orbital timescale, $T_{\rm orb}$, in comparison to a characteristic radiation-reaction timescale, $T_{\rm rr}$. For the latter, we can use the timescale associated with the rate of change of the semilatus rectum, p, related to the pericenter distance by $r_p = p/(1 + e)$, namely, $T_{\rm rr} \sim p/|dp/dt|$. The radiation-reaction timescales of the other orbital elements are comparable or larger (see, e.g., Glampedakis 2005). The ratio of these timescales is

$$\frac{T_{\rm orb}}{T_{\rm rr}} \sim 2\pi\mu\left(\frac{R_\bullet}{2p}\right)^{5/2}, \tag{3}$$

where $\mu = m/M_\bullet$ is the mass ratio of the system and m the SCO mass. It is evident that the radiation-reaction timescale is much greater than the orbital timescale due to the extreme mass ratio, $\mu \ll 1$, and because EMRBs have $p \gg \mu^{5/2} R_\bullet$. In the unlikely case that more accuracy is required, one could improve the analysis through the use of "Kludge" waveforms (Babak et al. 2007), which have been shown to reproduce numerical results in the adiabatic approximation accurately for EMRIs.

Formally, the orbital timescale used is not really the exact timescale of orbital motion. This is because the mass distribution of a MBH-embedded galaxy possesses a non-Keplerian potential that leads to non-Keplerian orbits. However, most EMRBs (by rate) have apocenters that do not extend far into the stellar population, implying that the contribution from the galaxy potential is minimal. The orbits we study in later sections have a contamination from the galactic potential that is less than 2% of the MBH mass. Moreover, Hopman et al. (2006) rightly argue that the inner region is statistically empty of stars, which is due to finite effects realized at the small scales observed near the MBH.

Certain constraints may be derived on the size of p and r_p for EMRB events. The most important constraint is derived from the definition of EMRBs: orbits with sufficiently large orbital period $T_{\rm orb} > T_{\rm cut}$. Assuming a Keplerian orbit (which is a rough assumption), this constraint translates to pericenter distances as follows:

$$r_p > (7.98 \times 10^{-7}\ {\rm pc})\frac{(1-e)}{0.1}\left(\frac{M_\bullet}{M_{\rm MW}}\right)^{1/3}\left(\frac{T}{T_{\rm cut}}\right)^{2/3}, \tag{4}$$

where we have rescaled quantities assuming a typical eccentricity of $e = 0.9$ (Rubbo et al. 2006a, 2006b) and a typical MBH mass of $M_\bullet = M_{\rm MW}$. In terms of geometrized units, such a constraint translates roughly to $r_p > 2R_\bullet$.

This constraint can be compared with the requirement that the SCO does not get captured. Any object that enters the black hole event horizon is captured, where the horizon is located (in Boyer-Lindquist coordinates) at

$$r_{\rm cap} = (1.91 \times 10^{-7}\ {\rm pc})\frac{M_\bullet}{M_{\rm MW}}\left[1 + \sqrt{1 - \frac{a_\bullet^2}{M_\bullet^2}}\right], \tag{5}$$

where $a_\bullet$ is the (Kerr) MBH spin parameter, related to its intrinsic angular momentum by $S_\bullet = GM_\bullet(a_\bullet/c)$, and bounded by $a_\bullet/M_\bullet \leq 1$. Thus, for a maximally spinning Kerr MBH ($a_\bullet = M_\bullet$), $r_{\rm cap} = 0.5R_\bullet$, while for a Schwarzschild (nonspinning) MBH it is just $R_\bullet$. This condition tell us simply that $r_p > r_{\rm cap}$, which is a condition superseded by the constraint on the orbital period given in equation (4). One could explore other possible constraints (Rubbo et al. 2006a, 2006b), but they are in general superseded by equation (4).

These constraints clearly exclude the ergosphere of the MBH ($r_{\rm cap} < r \lesssim R_\bullet$) where frame dragging effects are most pronounced. However, for EMRIs it has been argued (Glampedakis 2005) that orbits with $r_p < 10R_\bullet$ cannot be considered Keplerian anymore, mainly due to precessional effects. This statement can be made more quantitative by looking at the ratio of first-order post-Newtonian (1 PN) predictions (Blanchet 2006) to Newtonian ones (0 PN). For example, for the energy of a circular orbit, this ratio scales as $7R_\bullet/(8r_p)$, while for the perihelion precession angle, the ratio scales as $3R_\bullet/(2r_p)$, for extreme mass ratios. Therefore, for orbits with pericenter passage $r_p \sim 5R_\bullet$, the 1 PN correction to the energy and the perihelion precession angle is approximately 20% and 30%, respectively, relative to the Newtonian value. This indicates that, even for orbits outside the ergosphere, relativistic effects are not necessarily negligible.

The relativistic geodesic equations of motion introduce corrections to the Newtonian motion that can be interpreted in terms of a black hole *effective* potential. By comparing the Newtonian and relativistic potentials one can see that the relativistic corrections dominate over the centrifugal barrier at small distances from the black hole center. In this work we show that these relativistic corrections can be sampled by EMRBs and hence, one should model these systems accordingly. Nevertheless, as we argued above, the relativistic treatment of EMRBs does not need to be as sophisticated as in the case of EMRIs, since radiation reaction can be neglected.

3. EMRB WAVEFORMS

In this section we describe how we extract gravitational waveforms once we have integrated the geodesic equations of motion. We use a multipole-moment wave generation formalism for slowly moving objects with arbitrarily strong internal gravity (Thorne 1980; Flanagan & Hughes 2005; Glampedakis 2005). In quasi-Newtonian and semirelativistic treatments, the radiation is modeled by the lowest nonvanishing multipole moment: the mass quadrupole. To that order, and for the case of a pointlike object orbiting a MBH at a fixed coordinate location, the plus and cross polarizations are given by (Misner et al. 1973; Thorne 1980)

$$h_{+,\times} = \frac{2Gm}{rc^4}\epsilon^{ij}_{+,\times}(a_i z_j + v_i v_j), \tag{6}$$

where r is the (flat space) distance to the observer and $\epsilon^{ij}_{+,\times}$ are polarization tensors. This expression assumes, based on the slow-motion approximation, that the change in the acceleration with respect to time, the *jerk*, $j^i = da^i/dt$, is a small quantity. More precisely, we are neglecting terms of order $(v/c)^3$, or, in other words, since the (quadrupole) leading order terms are of order $(v/c)^2$, this implies a relative error of order v/c.

One can improve on this description for the gravitational radiation by accounting for higher order multipole moments. In this paper we consider the mass-octopole and current-quadrupole multipoles, which require the knowledge of one more time derivative of the trajectory, the jerk. Adding these contributions to equation (6), the gravitational waveforms are given by (Thorne 1980)

$$h_{+,\times} = \frac{2Gm}{rc^4}\epsilon^{ij}_{+,\times}\left\{a_i z_j + v_i v_j + \frac{1}{c}\left[(\boldsymbol{n}\cdot\boldsymbol{z})(z_i j_j + 3a_i v_j) + (\boldsymbol{n}\cdot\boldsymbol{v})(a_i z_j + v_i v_j) - (\boldsymbol{n}\cdot\boldsymbol{a})v_i z_j - \frac{1}{2}(\boldsymbol{n}\cdot\boldsymbol{j})z_i z_j\right]\right\}, \quad (7)$$

where $n^i = x^i/r$ is a unit vector that points to the observer and the vector product is the flat-space scalar product. In this case, we are neglecting terms of order $(v/c)^4$ and hence we are making a relative error of order $(v/c)^2$ with respect to the leading order quadrupole term.

The waveforms of equation (7) are a truncated multipole expansion, where we are neglecting the current-octopole, mass-hexadecapole, and higher multipole moments. This expansion is based on a slow-motion approximation which is valid for orbits whose pericenter velocity is small relative to the speed of light. For closed circular orbits, we can use the virial theorem to argue that this is equivalent to requiring $r_p > M_\bullet$. For a relativistic EMRB event with $v_p/c = 0.4$, the maximum relative contribution of the octopole to the quadrupole is of the order of 40%, since the octopolar term is of order v/c smaller than the quadrupolar one. In this paper we study EMRBs from the sample of Milky Way sources studied in Rubbo et al. (2006a). These sources have initial pericenter distances of $r_p > 8M_\bullet$, thus justifying the use of a low-multipolar expansion in the wave generation formalism and the neglect of radiation reaction effects in the orbital motion.

4. NUMERICAL SIMULATIONS

In this section we describe the EMRB simulations that were carried out, including the choice of initial conditions. The simulations involve integrating the equations for geodesic motion around a Kerr black hole, equation (2), forward in time. (For a detailed exposition of Kerr geodesics, see Chandrasekhar 1992.) Since Cartesian Kerr-Schild coordinates are used, the initial conditions can be denoted by (z_0^i, v_0^i). The numerical implementation does not use the Kerr geodesic constants of motion (energy, angular momentum, and Carter constant) in order to reduce the number of variables of the resulting system of ordinary differential equations. Instead, we have used the constants of motion to monitor the accuracy of the time integration. The integration accuracy is set so that we obtain fractional errors for the constants of motion smaller than one part in 10^{10}. The code uses a Bulirsh-Stoer extrapolation method as the evolution algorithm (see, e.g., Press et al. 1992; Stoer & Bulirsch 1993). We have also introduced in the code the possibility of switching between Kerr geodesics and Newtonian equations of motion. The gravitational waveforms are then obtained directly by applying expressions (6) and (7) to the numerically obtained trajectory $z^i(t)$.

Comparisons are carried out by choosing a representative relativistic orbit within the allowed phase space for EMRBs. We made the following choices for the test case:

1. The central MBH mass is $M_\bullet = M_{\rm MW}$ and the SCO mass is $m = 1\ M_\odot$, such that the mass ratio is $\mu = m/M_\bullet = 2.5 \times 10^{-7} \ll 1$.

2. The MBH spin parameter is either $a_\bullet = 0$ (Schwarzschild) or $a_\bullet = 0.998M_\bullet$ (Kerr). The angular momentum is aligned along the z-axis and equal to either $S^z = 0$ or $S^z = 0.998GM_\bullet^2/c$.

3. The observer is located at $r_{\rm obs} = 8$ kpc along the z-axis, which corresponds to the approximate distance from Earth to the center of the Milky Way (Eisenhauer et al. 2005).

Furthermore, we make the following choices for the orbital initial conditions:

$$z_0^i = (-1.59, 1.05, -0.185) \times 10^{-5}\ \text{pc},$$
$$v_0^i = (1.70, -2.89, 0.510) \times 10^4\ \text{km s}^{-1}. \quad (8)$$

The initial conditions are such that $r_0 = |z_0^i| = 50R_\bullet = 1.91 \times 10^{-5}$ pc, and $|v_0^i| = 0.11c = 3.39 \times 10^4$ km s^{-1}. The orbital plane is inclined by 10° with respect to the x-y plane to demonstrate the effects of orbital plane precession, which only occurs for spinning MBHs. Since this paper is concerned with the effect of relativistic corrections to EMRB events, we choose to give all orbits the same initial conditions. The possibility of relaxing this choice and its effect on the conclusions derived in this paper are discussed in a later section.

Although the test orbit is in the phase space of EMRB events studied in Rubbo et al. (2006a), one might worry that it is too relativistic to actually have a significant probability to occur in nature. In particular, one can think that the SCO may be tidally disrupted. To address this question, let us consider a Newtonian description of the central potential, which leads to the following values of the pericenter distance and velocity:

$$r_p = 6.45R_\bullet = 2.48 \times 10^{-6}\ \text{pc},$$
$$|v_p| = 0.384c = 1.15 \times 10^5\ \text{km s}^{-1}. \quad (9)$$

One might worry that stars might be tidally disrupted with such small pericenters. However, as shown by Hopman et al. (2006) most SCOs in EMRB scenarios consist of stellar-mass black holes, which cannot be tidally disrupted.

Such relativistic orbits are actually naturally occurring in the phase space of possible EMRBs studied in Rubbo et al. (2006a). Of all orbits in the allowed EMRB phase space considered in Rubbo et al. (2006a, 2006b) 6% are contained within a small six-dimensional phase-space volume centered on the test orbit.[1] Furthermore, the test case shown possesses a short orbital timescale, bursting approximately 150 times per year. Such events with small orbital timescale were shown to dominate the EMRB event rate in Rubbo et al. (2006a). It is in this sense that the test orbit studied here is *typical* or representative of EMRBs.

The relative location of the test orbit in the pericenter distance–eccentricity plane of the phase space of allowed EMRBs (Rubbo et al. 2006a) is presented in Figure 1 (*triangle*). The eccentricity was here calculated assuming a Newtonian orbit, and the pericenter separation is given in gravitational radii, $R_\bullet$. Although the test orbit has a large eccentricity, its apocenter is small enough ($r_a \lesssim 150R_\bullet \approx 6 \times 10^{-5}$ pc) that the contribution from the surrounding stellar population to the potential can be neglected. In general, the left side of the figure corresponds to highly relativistic orbits with large pericenter velocities and small pericenter

[1] In other words, 6% of the test orbits considered to be EMRBs in Rubbo et al. (2006a) are close in phase space to our test orbit. This does not imply that the probability of such a test orbit actually occurring in nature is 6%, since any element of phase space may have small overall probabilities, even down to 10^{-7}%.

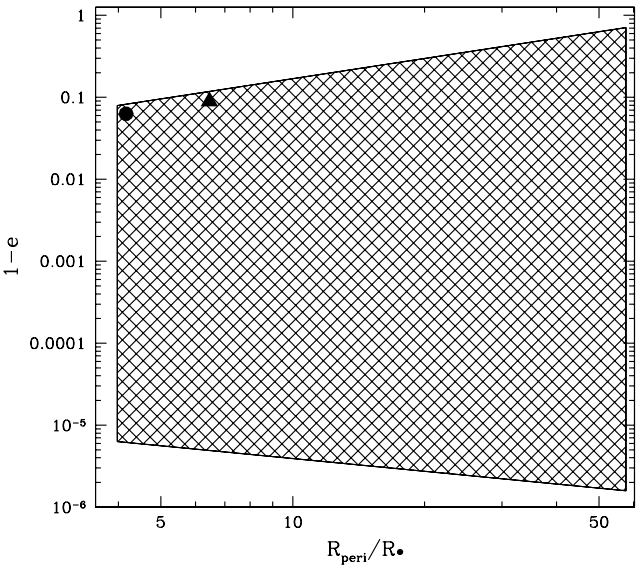

FIG. 1.—Set of possible EMRB orbits as computed in Rubbo et al. (2006a) in the pericenter distance–eccentricity plane. The pericenter distance is given in units of the gravitational radius $R_\bullet$. The initial conditions for the test (eq. [8]) and the extreme (eq. [10]) orbits are indicated by a triangle and a circle, respectively.

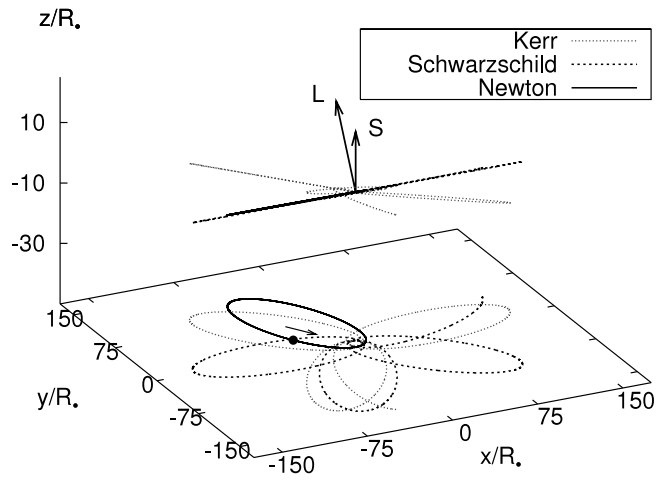

FIG. 2.—Trajectories for the SCO, with initial conditions given by eq. (8), corresponding to a Newtonian description (*solid line*) and relativistic descriptions with no spin (*dashed line*) and with spin (*dotted line*). The MBH is located at the origin, and the vectors L and S denote the initial orbital angular momentum and the MBH spin, respectively.

distances. Orbits with pericenter velocities $|v_p| > 0.25c = 3 \times 10^4$ km s^{-1} account for approximately 50% of the possible orbits within the phase space studied in Rubbo et al. (2006a).

Although the test orbit is a good source to demonstrate the differences between the Newtonian and relativistic treatments, we could have chosen an even more relativistic one. Such an event would still be classified as an EMRB in a Newtonian treatment, but it would border with the definition of a continuous source. An example of such an extreme orbit is shown with a circle in Figure 1, to the left of the test orbit (*triangle*). This extreme orbit possesses the following initial conditions:

$$z_0^i = (-1.81, 0.6, -1.06) \times 10^{-6} \text{ pc},$$
$$v_0^i = (1.72, -1.78, 0.31) \times 10^5 \text{ km s}^{-1}, \qquad (10)$$

where $r_p = 4R_\bullet = 1.53 \times 10^{-6}$ pc and $|v_p| = 0.49c = 1.46 \times 10^5$ km s^{-1} for a Newtonian potential. We study such an extreme orbit at the end of the next section as an example of a limiting relativistic case.

5. COMPARISON OF TRAJECTORIES AND WAVEFORMS

In this section we compare the results obtained for both the orbital motion and the gravitational radiation emitted by an EMRB event using both the Newtonian and relativistic description. Since the *plus* and *cross* polarization waveforms present similar features, we only plot the plus polarization waveforms. In the remainder of this section we use the following nomenclature: a quadrupolar (octopolar) Newtonian waveform is one that was calculated using the quadrupole (octopole) formula and Newtonian equations of motion; a quadrupole (octopole) Schwarzschild waveform is one that was calculated using the quadrupole (octopole) formula and the geodesic equations of motion with no spin ($a_\bullet = 0$); a quadrupole (octopole) Kerr waveform is one that was calculated using the quadrupole (octopole) formula and the geodesic equations of motion with spin $a_\bullet = 0.998M_\bullet$.

5.1. *Orbital Trajectories*

Let us begin by comparing the trajectories obtained in our simulations. In Figure 2 we plot the test orbit corresponding to a Newtonian treatment (*solid line*) and the one corresponding to a relativistic treatment without spin (*dashed line*) and with spin (*dotted line*). The dot and arrow indicate the initial location and velocity projected onto the x-y plane. The MBH is located at the origin of the coordinates, and the vectors denoted by L and S describe the direction of the initial orbital angular momentum and the MBH spin, respectively. In the relativistic description there are precessional effects in the SCO orbit that can be clearly observed in Figure 2. These precessional effects are pericenter precession about the orbital angular momentum axis, which acts in the initial orbital plane; and frame-dragging precession about the total angular momentum axis, which acts out of the initial orbital plane. While the former always occurs in a relativistic treatment, the latter is present only in the spinning case.

Different relativistic precessional effects are generally of different magnitude. These effects are usually inversely proportional to the pericenter distance, or equivalently proportional to the pericenter velocity of the SCO. Precession out of the initial orbital plane, however, is smaller than precession in the orbital plane by a relative factor of order v_p/c, and it is directly proportional to the spin of the MBH. In terms of post-Newtonian theory (see, e.g., Blanchet 2006), the pericenter advance is described by first-order post-Newtonian corrections to the equations of motion [order $(v/c)^2$ relative to the Newtonian acceleration], while precession off the orbital plane is due to spin-orbit and spin-spin couplings that correspond to 1.5 and second-order corrections [order $(v/c)^3$ and $(v/c)^4$ relative to the Newtonian acceleration]. Therefore, since EMRBs are characterized as events with small to moderate pericenter velocities, precession out of the initial orbital plane is small to moderate relative to pericenter advance, even for maximally spinning MBHs.

We can estimate the precession rate by comparing the Newtonian and relativistic trajectories. For the test orbit considered, we find that the rate in the orbital plane is roughly $\pi/3$ rad per orbit for the nonspinning case and $2\pi/3$ rad per orbit for the spinning one. These precessional effects have been studied extensively in the context of EMRIs (see, e.g., Schmidt 2002) and also specifically for S stars in the central region of our Galaxy in Kraniotis (2007). Nonetheless, these effects have not been previously analyzed in the context of EMRBs, since previous studies employed a quasi-Newtonian treatment.

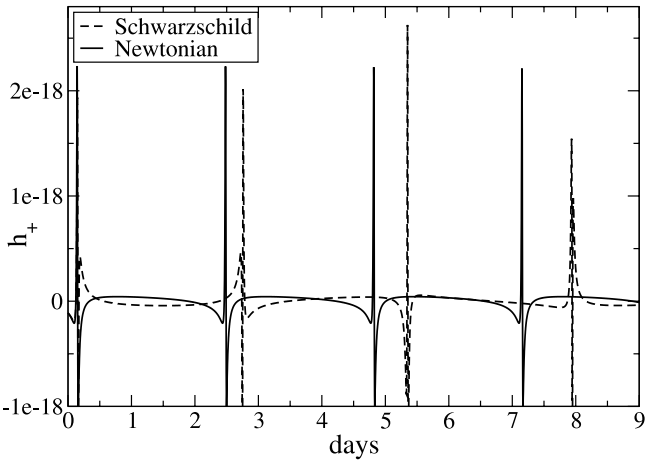

FIG. 3.—EMRB waveforms (plus polarization): the Newtonian waveform corresponds to the solid line and the Schwarzschild one to the dashed line. [*See the electronic edition of the Journal for a color version of this figure.*]

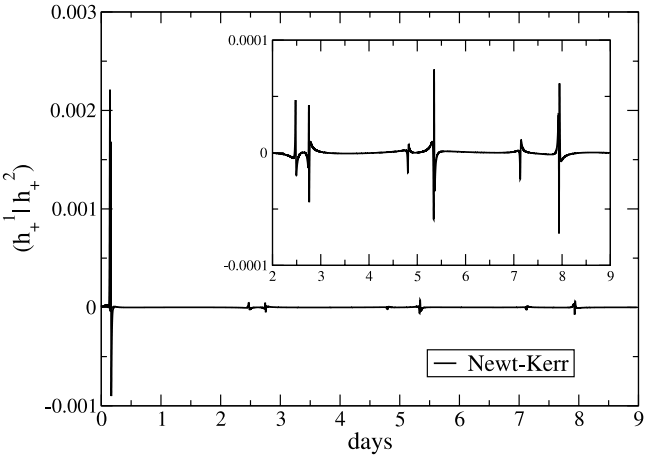

FIG. 5.—Overlap integrand of eq. (11) with h_1 given by the quadrupole Kerr waveform and h_2 by the quadrupole Newtonian one. The inset zooms to a region near the small peaks.

5.2. *Waveforms*

Let us now analyze how the differences in the SCO trajectories translate into different signatures in the waveforms. In Figure 3 we plot the quadrupole Newtonian and Schwarzschild waveforms (*solid and dashed lines, respectively*), while in Figure 4 we plot the quadrupole Schwarzschild and Kerr waveforms (*dashed and double-dot-dashed lines, respectively*). There are three main differences between the Newtonian and the relativistic waveforms: a modulated phase change, an amplitude change, and a time of arrival change. The changes in amplitude and time of arrival are due to the test particle experiencing a larger "force" of attraction as it approaches the black hole. Quantitatively, this increase in force is due to the presence of (r_p^{-n})-contributions to the relativistic corrections to the central potential (with n a real positive number).

Gravitational wave interferometers are most sensitive to the phase, which is clearly different for Newtonian and relativistic waveforms. The dephasing present in Figures 3 and 4 parallels the orbital dephasing discussed earlier (the gravitational wave and orbital frequencies are intimately related) and leads to an amplitude modulation. In terms of the gravitational wave phase, both Figures 3 and 4 show a dephasing of $\pi/6$ rad per cycle. This can be seen after the third burst where the waveforms are back in phase. In fact, there is a significant dephasing even between the relativistic waveforms due to the effect of the MBH spin. If a cursory examination by eye can detect the difference in the waveforms due to differences in the nature of the central potential, it stands to reason that strong-field EMRB waveforms might allow us to probe of the spacetime near a MBH. We should note, however, that no work has yet been done to find best-fit parameters for Newtonian waveforms that maximize the correlation with relativistic ones. In other words, it might be possible to mimic some of the relativistic corrections by choosing different initial data for the Newtonian waveforms, but such a study is beyond the scope of this paper.

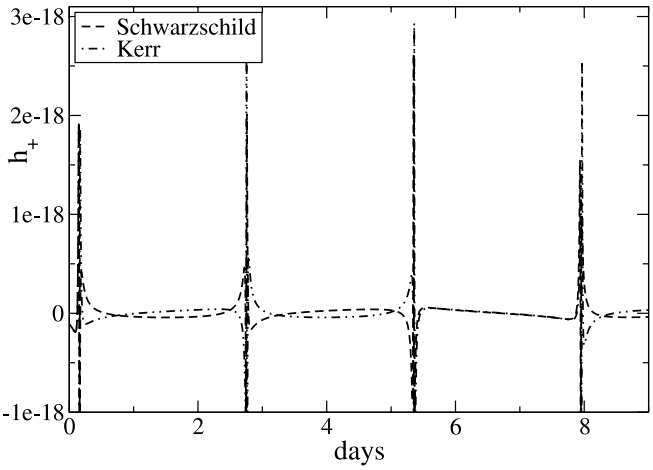

FIG. 4.—EMRB waveforms (plus polarization): the Schwarzschild waveform corresponds to the dashed line and the Kerr one to the double-dot-dashed line. The dephasing of the waveforms can be best observed during the silent transitions between bursts. For example, in the first silent transition the waveforms are roughly π radians out of phase, while in the third one they are in phase. [*See the electronic edition of the Journal for a color version of this figure.*]

The difference in dephasing can be better studied by calculating the signal overlap,

$$(h_1|h_2) = \frac{\int_0^T h_1(t)h_2(t)\,dt}{\sqrt{\int_0^T h_1^2(t)\,dt}\sqrt{\int_0^T h_2^2(t)\,dt}}. \qquad (11)$$

The overlap indicates how well a signal h_1 can be extracted via matched filtering with a template h_2.[2] In Figures 5 and 6 we plot the normalized integrand as a function of time, with h_1 given by the quadrupole Kerr waveform and h_2 given by either the quadrupole Newtonian or Schwarzschild waveforms. Observe that neither the Newtonian nor the Schwarzschild waveforms match well with the Kerr waveform. Moreover, note that the correlation with the Newtonian waveform deteriorates greatly after only the first cycle. The integral of equation (11) gives the correlation between different waveforms over 9 days (four bursts): for the Newtonian and Kerr plus-polarized waveforms it is 9.6%; for the Schwarzschild and Kerr plus-polarized waveforms it is -6.3%. As a point of comparison, a substantial signal overlap should be $\gtrsim 95\%$. As already mentioned, the same initial conditions were chosen for both the Newtonian and relativistic orbits, such that their waveforms would be both initially in-phase and any dephasing due to relativistic effects could be clearly studied. However, such a choice forces the SCO to pass through periapsis at slightly different times, because in the relativistic case this object

[2] The overlap is given here in the time domain, but an analogous representation in the frequency domain could also be used. Such an expression in the frequency domain can be derived through Parseval's theorem.

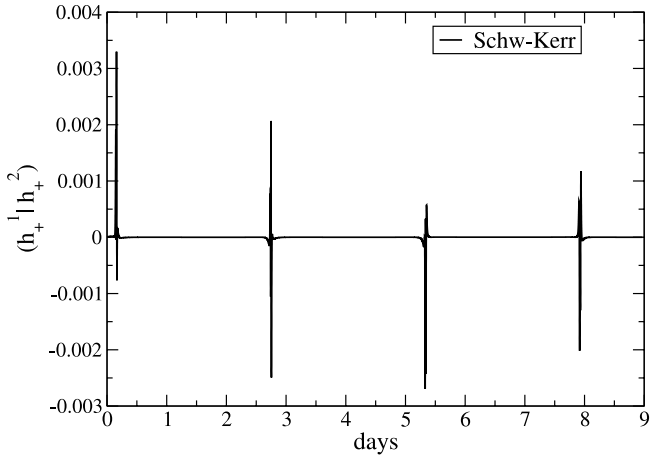

FIG. 6.—Overlap integrand of eq. (11) with h_1 given by the quadrupole Kerr waveform and h_2 by the quadrupole Schwarzschild one.

experiences a "deeper" potential. Such a difference in timing degrades the overlap somewhat and could, in principle, be ameliorated by choosing different initial conditions for the Newtonian evolution, i.e., by maximizing the overlap over all orbital parameters, but such a study is beyond the scope of this paper.

Figures 5 and 6 provide some evidence that the use of a relativistic waveform might be required for the data analysis problem of extracting EMRB signals. Such expectations are somewhat confirmed in Table 1, where we present the correlation between Newtonian and Kerr plus-polarized waveforms integrated over both a single day (one burst) and 9 days of data (several bursts) for a sample of different EMRB orbits.[3] Both a single and several bursts should be studied because, in principle, parameter adjustments might mitigate the between-burst dephasing, but probably not the in-burst dephasing. The orbits chosen were taken directly from the allowed EMRB phase space of Rubbo et al. (2006a) and possess different initial positions and velocities, leading to different eccentricities, initial inclination, and orbital periods. The orbital period can be used to classify the orbits into highly bursting (burst more than once per week) and slowly bursting (burst less than once per week.) For highly bursting EMRBs, the average correlation is ~27% when all 9 days of data (several bursts) are used, while it is ~93% when only 1 day of data (single burst) is used. For the slowly bursting EMRBs we considered here, there is actually only one burst per week, and its correlation is ~85%. These results indicate that accumulating precession effects lead to a significant loss of correlation between Newtonian and Kerr waveforms if bursts are to be connected. Moreover, we see that even for a single burst the shape of the relativistic waveforms is sufficiently different from its Newtonian counterpart to lead to a significant mismatch (in-phase dephasing). If one maximizes the correlation over intrinsic orbital parameters it might be possible to increase the correlation somewhat, but again that is to be studied elsewhere.

Let us now focus on the differences in the waveforms when they are calculated with the quadrupolar approximation versus the quadrupolar-octopolar one. In Figure 7 we plot the absolute value of the difference between the octopole and quadrupole waveforms as a function of time for a Schwarzschild (*top*) and a Kerr (*bottom*) central potential. The difference is normalized to the maximum of the first peak of the quadrupole waveform, since other peaks have approximately the same maximum.

Observe that the inclusion of higher order multipoles does not affect the phasing of the waveforms, but only the amplitude, which is in general different by roughly 4% relative to the quadrupole waveform for the Kerr test case. At first sight, this result is in disagreement with the expectation that the octopolar correction is at most $\lesssim 40\%$ of the quadrupolar one. Note, however, that the 40% estimate is an order-of-magnitude *upper limit*, since the octopole correction is dependent on the location of the observer relative to the trajectory, velocity, acceleration, and jerk vectors. For the test case, where the observer is located on the $\hat{z}$-axis and the orbit is initially inclined by 10°, the octopolar change is reduced by

[3] Here we use the frequency representation of the correlation calculation, employing the Fourier transform of the waveforms.

TABLE 1
S/N AND OVERLAP FOR DIFFERENT EMRB ORBITS

r_p (μpc) (1)	v_p/c (2)	P (yr) (3)	e (4)	No. Bursts (5)	$\lvert\Delta\rho\rvert/\rho$ (6)	$\lvert\Delta\rho^{(1)}\rvert/\rho^{(1)}$ (7)	$(h_1\lvert h_2)$ (8)	$(h_1\lvert h_2)^{(1)}$ (9)
Highly Bursting								
7.8	0.196	0.0042	0.603	6	0.38	0.049	0.27	0.98
7.5	0.207	0.0055	0.684	5	0.13	0.0007	0.20	0.88
7.2	0.217	0.0074	0.749	4	0.22	0.057	0.31	0.90
7.1	0.220	0.0086	0.777	3	0.49	0.061	0.33	0.99
Slowly Bursting								
13	0.163	0.0450	0.859	1	...	0.002	...	0.90
8.0	0.217	0.1953	0.968	1	...	0.033	...	0.97
10	0.193	0.7683	0.984	1	...	0.009	...	0.72
12	0.173	3.0407	0.992	1	...	0.015	...	0.80

NOTES.—In this table we present the S/N and correlation computed in the frequency domain between Kerr quadrupole and octopole waveforms for different EMRB orbits. The orbits are separated into two groups: highly bursting and slowly bursting. The first five columns present information about the different orbits, including how many times they burst, their eccentricities and periods, which were chosen directly from the allowed EMRB phase space of Rubbo et al. (2006a) and thus represent Milky Way sources. The sixth and seventh columns present the difference in S/N between a Newtonian and Kerr quadrupole waveform relative to the former using the entire data set and only one burst, respectively. Similarly, the eighth and ninth columns show the correlation between the plus polarizations using the entire data set and one burst, respectively. Since the slowly bursting sources burst only once, the sixth and eighth columns are not redundant for these sources. All calculations assume the observer is located on the z-axis and random initial inclination angles.

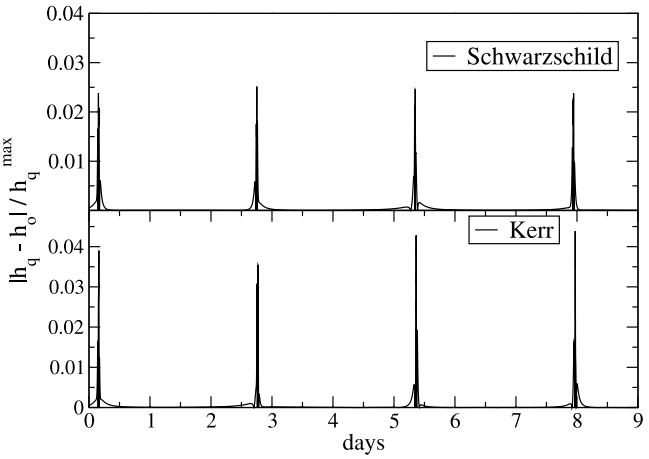

FIG. 7.—Absolute magnitude of the difference between the quadrupole and octopole Schwarzschild (*top*) and Kerr (*bottom*) waveforms. The difference is normalized to the maximum value of the first peak of the quadrupole waveform.

TABLE 2

COMPARISON BETWEEN QUADRUPOLE AND OCTOPOLE WAVEFORMS

Angle (deg)	x_{obs} (kpc)	y_{obs} (kpc)	z_{obs} (kpc)	Amp. Diff. (%)
0	0	0	8	3.9
20	2.73	0	7.51	3.3
40	5.14	0	6.12	11.5
60	6.93	0	4	15.2
80	7.88	0	1.39	19.7
100	7.88	0	−1.39	21.6
120	6.93	0	−4	17.8
140	5.14	0	−6.13	43.3
160	2.74	0	−7.52	8.6

NOTES.—Here we present an approximate measure of the amplitude difference between the quadrupole and octopole waveforms. We concentrate only on the first burst of radiation, and we normalize the difference to the maximum of the first peak of the quadrupole waveform. The difference is presented as a function of the observer location, which is always at a fixed radial distance of $r_{obs} = 8$ kpc, but rotated about the $\hat{y}$-axis on the $\hat{x}$-$\hat{z}$ plane (θ is here the usual Euler polar angle).

approximately an order of magnitude, since initially $(\boldsymbol{n}\cdot\boldsymbol{z}) \approx (\boldsymbol{n}\cdot\boldsymbol{v}) \approx (\boldsymbol{n}\cdot\boldsymbol{a}) \approx (\boldsymbol{n}\cdot\boldsymbol{j}) \approx 0.1$. In Table 2 we present the approximate maximum difference between octopolar and quadrupolar waveforms as a function of observer location, focusing only on the first burst of radiation. The location of the observer is rotated about the $\hat{y}$-axis on the $\hat{x}$-$\hat{z}$ plane, always at a fixed radial distance of 8 kpc. Note that for some observers the difference is larger and, in fact, of the order of 40%, since the dot products are closer to unity. These results are thus consistent with the expectation that the nth multipolar contribution cannot in general be larger than order $(v/c)^n$ relative to the quadrupolar leading term.

5.3. *Data Analysis*

In order to quantify some of our statements about the change in phase and amplitude, we calculated the S/N for the relativistic waveforms via the standard formula

$$\rho^2 = 4\int_0^\infty \frac{|\tilde{h}(f)|^2}{S_n(f)}\, df, \tag{12}$$

where the tilde denotes the Fourier transform and $S_n(f)$ is the one-sided power spectral noise density. Here we employ the Online Sensitivity Curve Generator (Larson et al. 2000) with the standard *LISA* settings and the inclusion of the white dwarf background contribution. When calculating S/Ns, we set the observation time to roughly 9 days, so as to include multiple bursts in our single S/N value.

The inclusion of relativistic corrections in the trajectories has a dramatic impact in the S/N. We find that the Schwarzschild waveform increases the S/N by a factor of approximately 59%, while the Kerr waveform increases it by 162%, relative to the Newtonian S/N. The difference in S/N is because the relativistic orbits experience a deeper effective potential and, thus, the interaction timescale is smaller. Therefore, the inverse of the interaction time, $f_\star = v_p/r_p$, is larger for the Schwarzschild and Kerr waveforms relative to the Newtonian one. As a result, the Fourier power is shifted to higher frequencies, where *LISA* is more sensitive.

The S/N behaves similarly for other EMRB orbits with different orbital periods, eccentricities, and pericenter parameters. This can be observed in Table 1, where we present the S/N difference between Newtonian and Kerr waveforms for different EMRB orbits for a single and several bursts. Highly bursting EMRBs lead to a large change in the S/N over a weak of data, since they experience the depths of the effective potential several times. Per burst, the change in S/N can range from 1% to 10% or even 90%, depending on the inclination angle of the orbit, the pericenter distance, and other orbital parameters. Also note that the orbits presented in the table are not as relativistic as the test case, which is why the S/N difference is smaller. This study seems to indicate that the S/N is in general somewhat larger for relativistic waveforms, especially when several burst are taken into account.[4] Consequently, the event rate calculated in Rubbo et al. (2006a, 2006b), which in particular summed over all bursts in 1 yr of data, is an underestimate for their galaxy model, because some of the systems with a Newtonian S/N $\lesssim 5$ should have been added to the detectable event rate. However, the uncertainty in the event rate is still probably dominated by astrophysical uncertainties and not by the dynamics modeling.

Conversely, the inclusion of higher multipole moments to the wave generation formalism has little to no effect in the S/N. In the previous section we showed that there was ≈4% difference between the octopole and quadrupole waveforms relative to the maximum of the first peak of the quadrupole waveform. We further showed that this difference depends on the location of the observer (see Table 2), but for the test case it does not exceed a maximum of 40%, which agrees with the multipole-ordering argument previously described. However, we also pointed out that the amplitude difference is confined to sharp peaks in the time domain. Such a confined change in the waveform amplitude leads to a Fourier power being dispersed over a large frequency region, including outside the *LISA* band. As a result, there is a correspondingly small change in the S/N: of the order of ≈1% relative to the quadrupolar formalism. Such a result is in agreement with the analysis of Babak et al. (2007) which was carried out for EMRIs. Therefore, we see that the change in S/N is primarily dominated by the modifications introduced in the geodesic description of the equations of motion, and not in the octopolar correction to the waveform generation.

The analysis presented in this section, in particular Figure 5, makes it clear that relativistic corrections to the waveforms accumulate with multiple bursts. In other words, over a single burst

[4] Naive intuition might suggest that the change in the S/N should scale like the square root of the number of bursts, but this is not necessarily correct. This is because these bursts start at frequencies very close to the limit of *LISA*'s sensitivity band (10^{-5} Hz). As the orbits burst, precession somewhat increases the frequency of the waveform, forcing different bursts to contribute different amounts to the S/N.

(pericenter passage), a quadrupolar waveform calculation using Newtonian dynamics might be sufficient. However, if one wants to estimate parameters associated with the central MBH, then multiple bursts might be necessary to associate the events to a single SCO trajectory. In terms of data analysis, for a detection search it is simpler to look for a single burst using techniques such as excess power and wavelet decompositions (e.g., see Anderson et al. 2001; Klimenko et al. 2004; Stuver & Finn 2006; Camarda & Ortolan 2006). For estimating MBH parameters, the results of this paper suggest that multiple bursts might have to be connected. For this to occur, a single template may be used, but as our results indicate, the template will need to incorporate the effects of general relativity.[5]

At this juncture, we should comment on some of the caveats in the conclusions derived from the analysis presented here. First, in this paper we have primarily concentrated on the question of characterizing the gravitational waves through the study of the S/N and overlap. In this study, however, we have not maximized these data analysis measures with respect to (intrinsic or extrinsic) orbital parameters. Although it might be possible to improve the S/N and overlap via parameter maximization, our study suggests that the introduction of relativistic effects, such as precession, lead to a clear imprint on the waveform that might be difficult to mimic with a purely Newtonian waveform irrespective of its parameters. Second, in this paper we have only touched the iceberg of the signal characterization and parameter estimation problem. A possible route to study this problem is through a numerical Fisher analysis, with the complications derived from the fact that the waveforms are known only numerically. Furthermore, increasing the complexity of the waveform will also increase the computational cost of these studies and, thus, it might be interesting to investigate whether it is possible or advantageous to search for individual bursts with similar frequency and identify them as belonging to the same physical system. These issues are beyond the scope of this paper, but they should be addressed in future investigations.

Setting these caveats momentarily aside, let us conclude with some discussion of the extreme relativistic case introduced earlier. As we have seen, relativistic corrections can introduce strong modifications to EMRB waveforms, which depend on how relativistic the EMRB event is and, in particular, on the pericenter velocity. The corrections are particularly strong for the class of EMRBs that inhabit the boundary between EMRBs and EMRIs, defined by the $T_{\rm cut} = 3 \times 10^4$ s value, corresponding to the period between apocenter passages. An example of such an event is the extreme orbit discussed in § 4, whose waveform is shown in Figure 8. Observe that a simplistic Newtonian description misses the rich structure, in which the SCO whirls twice about the black hole before zooming out to apocenter again. This behavior is missed entirely when we evolve the orbit with the Newtonian equations of motion, even though the same initial conditions were used. Even though in the previous cases a Newtonian waveform might be able to extract relativistic events by adjusting intrinsic parameters, such is definitely not the case for the highly relativistic event of Figure 8, since no choice of parameters in the Newtonian waveform can reproduce its multiple-peak structure.

Due to their whirling behavior, the extreme orbit waveform resembles the zoom-whirl events often mentioned in the EMRI literature (Hughes 2001a, 2001b; Glampedakis & Kennefick 2002). However, the event is still an EMRB and not an EMRI because the period between apocenter passages is too long. For our galactic model, we find the probability of a small region of phase space around this orbit to be rather high, 10%. If this EMRB is detected with sufficiently high S/N, it seems plausible that a parameter estimation analysis would allow for a determination of the background parameters, such as the black hole spin. Barack & Cutler (2004b) have already investigated *LISA*'s ability to measure MBH properties using approximate EMRI signals. They found that, depending on the actual orbital parameters, it will be possible to measure the MBH spin with fractional errors of 10^{-3} to 10^{-5}. This high-precision measurement is the result of observing up to $\sim 10^6$ complete orbits. Conversely, it is very unlikely that EMRB measurements will be able to match the measurement capabilities of EMRI signals, since only a few bursts will probably be available. Whether accurate parameter extraction is possible can only be determined with a more detailed data analysis investigation of EMRBs.

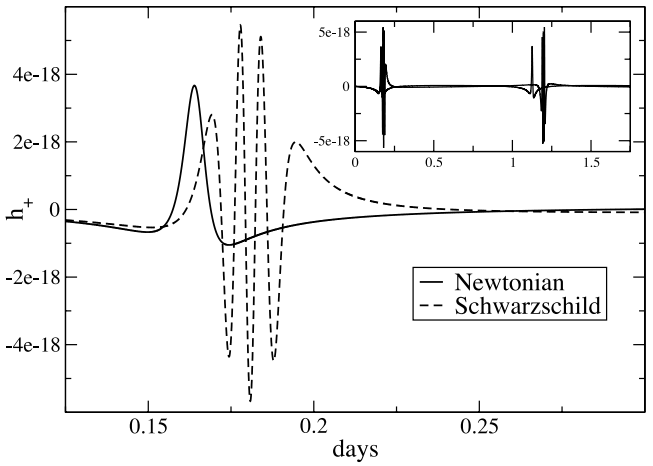

FIG. 8.—Plot of the quadrupole Newtonian (*solid line*) and Schwarzschild (*dashed line*) gravitational waveform as a function of time. [*See the electronic edition of the Journal for a color version of this figure.*]

6. CONCLUSIONS

We have studied the effects of relativistic corrections on the gravitational waves produced by EMRBs. These events originate from long-period orbits of a SCO around a MBH, leading to large-amplitude, quasi-periodic gravitational wave bursts. Using a more accurate relativistic treatment of the phenomenon, we have improved on the waveforms and trajectories relative to previous work. The orbital trajectories were corrected by accounting for the spacetime curvature of the system for Schwarzschild and Kerr MBHs. The waveform generation was corrected by accounting for the next-order term in the multipolar expansion of gravitational radiation.

We found that relativistic corrections change the waveform shape relative to its Newtonian counterpart. One of the most significant changes was found to be an amplitude-modulated dephasing, produced by the relativistic corrections to the orbital trajectory and, in particular, by relativistic precessional effects. Other effects included a change in the amplitude of the waveform, partially produced by the inclusion of higher order terms in the gravitational wave generation scheme.

The magnitude of the relativistic corrections was found to be directly proportional to the pericenter velocity of the orbit, as expected. Surprisingly, we estimated that at least 50% of the orbits analyzed in Rubbo et al. (2006a, 2006b) acquire relativistic

[5] A note of caution should be added here, since a detailed study of the maximization of the overlap with respect to orbital parameters in the Newtonian waveform has not yet been carried out. Indeed, it might be possible to mimic some of the relativistic effects with Newtonian waveforms with varying parameters, but such mimicking is most probably not possible for highly relativistic EMRBs.

velocities and, thus, nonnegligible relativistic corrections. We investigated these corrections in detail by choosing a test orbit that is representative of the kind that dominated the event rate calculation of Rubbo et al. (2006a). We also studied a limiting case of a highly relativistic EMRB and found that it whirls more than once around the MBH before zooming back to apocenter and becoming silent again.

We have also discussed the possible consequences that relativistic effects might have on the detection and parameter estimation of gravitational waves from EMRBs by *LISA*, namely, a change in the S/N and loss of overlap. These changes are mainly due to the relativistic treatment of the equations of motion, while a quadrupolar wave generation formalism seems to suffice. This finding is relevant particularly to match filtering searches, where a Newtonian treatment of the orbit might lead to a deterioration of confidence limits. Furthermore, our study suggests that, given an EMRB gravitational wave detection, it might be plausible to extract or bound the spin of the central potential with a template that takes into account the Kerr character of the MBH. Other astrophysical consequences include a possible increase in the event rate, which implies that the rates of Rubbo et al. (2006a, 2006b) and Hopman et al. (2006) might be lower limits, although these estimates are still dominated by uncertainties in the astrophysical modeling for the host galaxy.

In addition to the astrophysical modeling, future research should tackle the details of the EMRB data analysis and signal extraction issues put forward above. Based on the results of this paper, one may explore the possibility of testing alternative theories of gravity with EMRBs by performing matched filtering with templates from alternative theories (Will 1998; Scharre & Will 2002; Will & Yunes 2004; Berti et al. 2005a, 2005b). Another possible avenue for future research is the study of the confidence limits with which the spin of the central MBH can be measured.

This research could then be used to examine whether EMRB events can distinguish between a pure Kerr MBH and some other spacetime. Such studies have already began with the analyses of Collins & Hughes (2004), Glampedakis & Babak (2006), and Barausse et al. (2007), where comparisons between a Kerr and other non-Kerr spacetimes were performed. Such studies could be extended to the perturbed Kerr solution found by Yunes & Gonzalez (2006), where the perturbation is parameterized by the Weyl tensor of the external universe and could represent some external accretion disk, planetary system, or some other compact object. Ultimately, these investigations will decide whether EMRB events are worth studying in further detail by future gravitational wave observatories.

The authors would like to thank Ben Owen for reading the manuscript and providing useful comments, as well as the anonymous referee for providing insightful suggestions. We would also like to acknowledge the support of the Center for Gravitational Wave Physics funded by the National Science Foundation under Cooperative Agreement PHY-01-14375, and support from NSF grants PHY 05-55628, PHY 05-55436, PHY 02-18750, PHY 02-44788, PHY 02-45649, and PHY 00-99559. K. H. B. and L. R. also acknowledge the support of NASA NNG04GU99G and NNG05GF71G. C. F. S. acknowledges the support of the Natural Sciences and Engineering Research Council of Canada.

REFERENCES

Amaro-Seoane, P., et al. 2007, preprint (astro-ph/0703495)
Anderson, W. G., Brady, P. R., Creighton, J. D. E., & Flanagan, E. E. 2001, Phys. Rev. D, 63, 042003
Babak, S., Fang, H., Gair, J. R., Glampedakis, K., & Hughes, S. A. 2007, Phys. Rev. D, 75, 024005
Barack, L., & Cutler, C. 2004a, Phys. Rev. D, 70, 122002
———. 2004b, Phys. Rev. D, 69, 082005
Barausse, E., Rezzolla, L., Petroff, D., & Ansorg, M. 2007, Phys. Rev. D, 75, 064026
Bender, P., et al. 1998, *Laser Interferometer Space Antenna* for the Detection and Observation of Gravitational Waves: An International Project in the Field of Fundamental Physics in Space, Pre-Phase A Report (Garching: MPQ)
Berti, E., Buonanno, A., & Will, C. M. 2005a, Phys. Rev. D, 71, 084025
———. 2005b, Classical Quantum Gravity., 22, S943
Blanchet, L. 2006, Living Rev. Relativ., 9, 4
Camarda, M., & Ortolan, A. 2006, Phys. Rev. D, 74, 062001
Chandrasekhar, S. 1992, The Mathematical Theory of Black Holes (New York: Oxford Univ. Press)
Collins, N. A., & Hughes, S. A. 2004, Phys. Rev. D, 69, 124022
Danzmann, K., & Rüdiger, A. 2003, Classical Quantum Gravity, 20, S1
Eisenhauer, F., et al. 2005, ApJ, 628, 246
Flanagan, E. E., & Hughes, S. A. 2005, New J. Phys., 7, 204
Gair, J. R., Kennefick, D. J., & Larson, S. L. 2005, Phys. Rev. D, 72, 084009
———. 2006, ApJ, 639, 999
Gair, J. R., et al. 2004, Classical Quantum Gravity, 21, S1595
Ghez, A. M., et al. 2005, ApJ, 620, 744
Glampedakis, K. 2005, Classical Quantum Gravity, 22, S605
Glampedakis, K., & Babak, S. 2006, Classical Quantum Gravity, 23, 4167
Glampedakis, K., & Kennefick, D. 2002, Phys. Rev. D, 66, 044002
Holley-Bockelmann, K., & Sigurdsson, S. 2006, MNRAS, submitted (astro-ph/0601520)
Hopman, C., & Alexander, T. 2006, ApJ, 645, L133
Hopman, C., Freitag, M., & Larson, S. L. 2006, MNRAS, submitted (astro-ph/0612337)
Hughes, S. A. 2001a, Phys. Rev. D, 64, 064004
———. 2001b, Classical Quantum Gravity, 18, 4067
Klimenko, S., Yakushin, I., & Mitselmakher, G. 2004, Classical Quantum Gravity, 21, S1685
Kraniotis, G. V. 2007, Classical Quantum Gravity, 24, 1775
Larson, S. L., Hiscock, W. A., & Hellings, R. W. 2000, Phys. Rev. D, 62, 062001
Marck, J.-A. 1996, Classical Quantum Gravity, 13, 393
Misner, C. W., Thorne, K., & Wheeler, J. A. 1973, Gravitation (San Francisco: Freeman)
Poisson, E. 2004, Living Rev. Relativ., 7, 6
Press, W. H., Flannery, B. P., Teukolsky, S. A., & Vetterling, W. T. 1992, Numerical Recipes: The Art of Scientific Computing (Cambridge: Cambridge Univ. Press)
Rubbo, L. J., Holley-Bockelmann, K., & Finn, L. S. 2006a, ApJ, 649, L25
———. 2006b, in AIP Conf. Proc. 873, *Laser Interferometer Space Antenna*: 6th International *LISA* Symposium, ed. S. M. Merkowitz & J. C. Livas (New York: AIP), 284
Ruffini, R., & Sasaki, M. 1981, Prog. Theor. Phys., 66, 1627
Scharre, P. D., & Will, C. M. 2002, Phys. Rev. D, 65, 042002
Schmidt, W. 2002, Classical Quantum Gravity, 19, 2743
Stoer, J., & Bulirsch, R. 1993, Introduction to Numerical Analysis (New York: Springer)
Stuver, A. L., & Finn, L. S. 2006, Classical Quantum Gravity, 23, S733
Sumner, T. J., & Shaul, D. N. A. 2004, Mod. Phys. Lett. A, 19, 785
Thorne, K. S. 1980, Rev. Mod. Phys., 52, 299
Tremaine, S., et al. 1994, AJ, 107, 634
Will, C. M. 1998, Phys. Rev. D, 57, 2061
Will, C. M., & Yunes, N. 2004, Classical Quantum Gravity, 21, 4367
Yunes, N., & Gonzalez, J. A. 2006, Phys. Rev. D, 73, 024010